Enantioseparation of planar chiral ferrocenes on cellulosebased chiral stationary phases: benzoate versus carbamate pendant groups

Roberto Dallocchio, Alessandro Dessì, Barbara Sechi, Bezhan Chankvetadze, Giorgi Jibuti, Sergio Cossu, Victor Mamane, Paola Peluso

Enantioseparation of planar chiral ferrocenes on cellulose-based chiral stationary phases: benzoate versus carbamate pendant groups

Roberto Dallocchio,[1,‡] Alessandro Dessì,[1,‡] Barbara Sechi,[1,‡] Bezhan Chankvetadze,[2] Giorgi Jibuti,[2] Sergio Cossu,[3] Victor Mamane,[4,*] and Paola Peluso[1,*]

[1] Enantioselective Chromatography and Molecular Recognition Unit, Istituto di Chimica Biomolecolare ICB CNR, Sede secondaria di Sassari, Sassari, Italy.

[2] Institute of Physical and Analytical Chemistry, School of Exact and Natural Sciences, Tbilisi State University, Tbilisi, Georgia.

[3] Dipartimento di Scienze Molecolari e Nanosistemi, Università Ca' Foscari Venezia, Mestre Venezia, Italy.

[4] Institut de Chimie de Strasbourg, UMR 7177, CNRS-Université de Strasbourg, Strasbourg, France.

[‡] These authors contributed equally to this work

*Correspondence should be addressed to the following authors:

Dr. Paola Peluso
Istituto di Chimica Biomolecolare, Consiglio Nazionale delle Ricerche
Traversa La Crucca 3, Li Punti, 07100 Sassari, Italy
paola.peluso@cnr.it

Dr. Victor Mamane
Institut de Chimie de Strasbourg, Centre National de la Recherche Scientifique and Université de Strasbourg
1 rue Blaise Pascal, 67008 Strasbourg Cedex, France
vmamane@unistra.fr

Keywords: Cellulose-based chiral stationary phases / enantiomer elution order / enantioseparation / molecular dynamics / planar chiral ferrocenes

Abbreviations: **CDMPC**, cellulose *tris*(3,5-dimethylphenylcarbamate); **CMB**, cellulose *tris*(4-methylbenzoate); **CSP**, chiral stationary phase; **EEO**, enantiomer elution order; **HB**, hydrogen bond; **MD**, molecular dynamics; **MeOH**, methanol; **MP**, mobile phase; **2-PrOH**, 2-propanol; ***V***, electrostatic potential; V_S, electrostatic potential

mapped on electron density isosurfaces; $\boldsymbol{V}_{\mathbf{S,max}}$, electrostatic potential maximum; $\boldsymbol{V}_{\mathbf{S,min}}$, electrostatic potential minimum; **vdW**, van der Waals; **XB**, halogen bond

Abstract

In this study, the enantioseparation of fourteen planar chiral ferrocenes containing halogen atoms, and methyl, iodoethynyl, phenyl and 2-naphthyl groups, as substituents, was explored with a cellulose *tris*(4-methylbenzoate) (CMB)-based chiral column under multimodal elution conditions. *n*-Hexane/2-propanol (2-PrOH) 95:5 v/v, pure methanol (MeOH), and MeOH/water 90:10 v/v were used as mobile phases (MPs). With CMB, baseline enantioseparations were achieved for nine analytes with separation factors (α) ranging from 1.24 to 1.77, whereas only three analytes could be enantioseparated with $1.14 \leq \alpha \leq 1.51$ on a cellulose *tris*(3,5-dimethylphenylcarbamate) (CDMPC)-based column, used as a reference for comparison, under the same elution conditions. Pendant group-dependent reversal of the enantiomer elution order (EEO) was observed in several cases by changing CMB to CDMPC. The impact of analyte and CSP structure, and MP polarity on the enantioseparation was evaluated. The two cellulose-based CSPs featured by different pendant groups were also compared in terms of thermodynamics. For this purpose, enthalpy ($\Delta\Delta H°$), entropy ($\Delta\Delta S°$) and free energy ($\Delta\Delta G°$) differences, isoenantioselective temperatures (T_{iso}) and enthalpy/entropy ratios (Q), associated with the enantioseparations, were derived from van't Hoff plots by using *n*-hexane/2-propanol 95:5 v/v and methanol/water 90:10 v/v as MPs. With the aim to disclose the functions of the different substituents in mechanisms and noncovalent interactions underlying analyte-selector complex formation at molecular level, electrostatic potential (V) analysis and molecular dynamics (MD) simulations were used as computational techniques. On this basis, enantioseparations and related mechanisms were investigated by integrating theoretical and experimental data.

1 Introduction

The interest of enantioseparation science toward chiral ferrocenes containing only a chiral plane as stereogenic unit is still in its infancy. Indeed, after the first chromatographic enantioseparations dating back to the 1980s [1,2], the most systematic analytical studies on the enantioseparation of planar chiral ferrocenes by HPLC [3-7], supercritical fluid chromatography [8], and CE [7] were published very recently. On one hand, this renewed interest toward planar chiral ferrocene

enantioseparations may be related to the growing attention of scientists toward this class of metallocenes for applications in fields like asymmetric synthesis [9], medicinal chemistry [10], chiroptical spectroscopy [11], and electrochemistry [12]. In this regard, it is worth mentioning that asymmetric synthesis procedures are not always able to provide enriched enantiomers with satisfactory enantiomeric excesses [13]. Thus, in these cases, the availability of efficient enantioseparation methods is essential for the development of the field, accessing pure or enriched enantiomers. This is particularly true for halogenated planar chiral ferrocenes given that they are versatile and valuable intermediates to access chiral ferrocenes with various functionalities [14-16]. On the other hand, studies on the enantioseparation of new chiral compounds may enable to acquire information on unusual and new chiral recognition mechanisms and related noncovalent interactions [5,6].

Although a few enantioseparations of planar chiral ferrocenes were performed by using CD-based [2,3] and brush-type [17] chiral columns, polysaccharide-based chiral stationary phases (CSPs) proved to be versatile platforms for the enantioseparation of ferrocene derivatives with planar chirality [13]. Indeed, despite the limited number of analytical studies performed in this field, over time enantioselective HPLC with polysaccharide-based chiral columns has been widely used by organic chemists to determine the enantiomeric excesses of planar chiral ferrocenes prepared by asymmetric synthesis procedures [13]. For this purpose, methylated, chlorinated and methylchlorinated polysaccharide carbamate-based CSPs were used in most cases [13], whereas cellulose benzoate-based chiral columns were exploited for a limited number of enantioseparations [8,18-20]. However, the cellulose *tris*(4-methylbenzoate) (CMB), as chiral selector, proved to be useful for the enantioseparation of planar chiral ferrocenes containing aromatic hydrocarbon frameworks [8,19].

Coated cellulose tribenzoate-based CSPs were developed in 1984 by the Okamoto group [21] and Ichida et al. [22]. In particular, CMB containing a methyl group, as electron-donor substituent of the phenyl ring, has shown high chiral recognition ability [23]. The versatility of this polymeric selector toward a wide range of racemates [24,25] is likely due to the high electron charge density of the carbonyl groups of the benzoate derivatives which is stabilized by the methyl substituent on the phenyl rings through

an inductive effect. Coated CMB-based chiral columns are commercially available under the trade names Chiralcel OJ (Daicel) and Lux Cellulose-3 (Phenomenex).

In recent studies performed by our groups, amylose-based selectors showed better performances compared to cellulose carbamate-based selectors for the enantioseparations of planar chiral ferrocenes **1**-**14** (Fig. 1), and only **3**, **4**, and **5** could be enantioseparated on cellulose *tris*(3,5-dimethylphenyl)carbamate (CDMPC) by using *n*-hexane/2-propanol (2-PrOH) 95:5 v/v (**3**, **4**) and methanol (MeOH)/water 90:10 v/v (**5**) as mobile phases (MPs) [4,5]. Moreover, amylose-based CSPs exhibited poor enantioseparation capability under normal phase elution conditions toward halogenated planar chiral ferrocenes which, rather, were enantioseparated better by using MeOH-containing MPs. Given the aromatic character of analytes **1**-**14**, the performances of CMB deserved to be explored with the aim to evaluate *a)* the versatility of this chiral selector towards the enantioseparation of chiral ferrocenes **1**-**14**, *b)* the impact of changing the pendant group (benzoate vs carbamate) of cellulose-based CSPs on these enantioseparations, *c)* if halogen bond (XB)-based enantioseparation could be identified.

On this basis, we reported herein the results of a systematic study on the HPLC enantioseparation of 1,2- and 1,3-disubstituted ferrocenes **1**-**14** with Lux Cellulose-3, as a CMB-based chiral column, and the Lux Cellulose-1, containing CDMPC, as reference for comparison (Supporting Information, Table S1), under multimodal elution conditions. The effect of temperature on the enantioseparations was considered, and thermodynamic quantities associated with the enantioseparations of ferrocenes **1**-**9** were derived from van't Hoff plots. In addition, the possible recognition mechanisms accounting for the differences in terms of enantioseparation capability of the two polymeric selectors were investigated through *a*) electrostatic potential (*V*) analysis [26,27] by mapping *V* values associated with the main interaction sites of selectors and of compounds **1**-**14** on electron density isosurfaces (V_S), and *b*) molecular dynamic (MD) simulations [28,29], virtually exploring the enantioseparation of ferrocene **3**, as test probe, with both CMB and CDMPC.

2 Materials and methods

2.1 Chemicals

Compounds **1**-**14** were prepared and characterized as previously reported [15,16,30,31]. HPLC grade *n*-hexane, ethanol, MeOH, 2-PrOH, ACN, and water were purchased from Sigma-Aldrich (Taufkirchen, Germany).

2.2 Chromatography

An Agilent Technologies (Waldbronn, Germany) 1100 Series HPLC system (high-pressure binary gradient system, a diode-array detector operating at multiple wavelengths (220, 254, 280, 360 nm), and a programmable autosampler with a 20 µl loop) was employed. Data acquisition and analyses were carried out with Agilent Technologies ChemStation Version B.04.03 chromatographic data software. The UV absorbance is reported as milliabsorbance units (mAU). Lux Cellulose-1 (CDMPC) and Lux Cellulose-3 (CMB), (5 µm) (Phenomenex Inc., Torrance, CA, USA) (Supporting Information, Table S1), were used as chiral columns (250 × 4.6 mm). Analyses were performed in isocratic mode at 25 °C if not indicated otherwise. The flow rate was set at 0.8 ml/min. For compounds **1**-**6**, and **9**, the enantiomer elution order (EEO) was determined by injecting enantiomers of known absolute configuration [5,16]. For compounds **7**, **8**, and **10**-**14**, the relative EEOs were assigned by injecting pure enantiomers of unknown absolute configuration which are denoted as $X_{\text{compound number}}$ and $Y_{\text{compound number}}$. The van't Hoff experiments were conducted at 5, 10, 15, 20, 25, 30, 35, and 40 °C by using a thermostat jacket equipped with a RE104 LAUDA circulating water-bath (Lauda, Königshofen, Germany) (resolution 0.1 °C; accuracy ±0.4 °C; temperature control ±0.02 °C). When the temperature was changed, the column was allowed to equilibrate for 1 h before injecting the samples. Thermodynamic parameters were derived from the slopes and the intercepts of the van't Hoff plots by linear regression analysis (see Supporting Information for details). Statgraphics Centurion 18 (Statpoint Technologies, Inc., Warrenton, VA, USA) was used for all linear regression analyses.

2.3 Computations

V extrema (maxima and minima) on the molecular electron density isosurfaces ($V_{S,max}$ and $V_{S,min}$) (au, electrons/bohr) were calculated by using Gaussian 09 (Wallingford,

CT 06492 USA) [32], at the density functional theory level of theory using the B3LYP functional and the def2-TZVPP basis set. Search for the exact location of $V_{S,max}$ and $V_{S,min}$ was made through the Multiwfn code [33] and through its module enabling quantitative analyses of molecular surfaces (isovalue 0.002 au) [34]. The .wfn files were obtained through the Gaussian 09 package. Details for MD are reported in the Supporting Information file.

3 Results and discussion

Along with the fact that the number and the position of the methyl groups featuring the pendant groups may also influence binding and enantiorecognition capability of the selector, the main difference between CDMPC (Fig. 2A) and CMB (Fig. 2B) is the absence of the amidic hydrogens (Fig. 2A, blue regions) in the benzoate-based selector. This feature has consequences at both intra- and intermolecular levels. Indeed, the pendant groups of the CMB contain exclusively carbonyl oxygens as hydrogen bond (HB) acceptors; intramolecular HBs stabilizing the highly-ordered structure of the polymer are thus not possible in this selector due to the lack of the amidic hydrogens, as HB donor counterpart. As a result, lower stability of the CMB compared to the phenylcarbamate derivative has been reported, and the chiral recognition properties of CMB are more influenced by the conditions used for the preparation of the packing material [21,35-37]. A comparison between computed nonameric (9-mer) models representing CDMPC and CMB (Fig. 2) shows that the benzoate-based polymer presents slightly smaller cavities than CDMPC, although they are reasonably more flexible for conformational adjustment due to the absence of intramolecular HBs featuring the structure.

At the intermolecular level, CMB is unable to behave as HB donor and, consequently, to form HBs with analytes having properties as HB acceptors. The electron charge density at the carbonyl oxygens of the CMB is expected to be higher compared to the corresponding sites of the CDMPC. To quantify this feature, the V_S on both carbamate and benzoate pendant groups was computed and compared (Supporting Information, Table S2). The $V_{S,min}$ value associated with the carbonyl oxygens is actually lower for the CMB compared to the CDMPC, confirming the superiority of the benzoate-based selector as HB acceptor. Moreover, a higher dipole associated to the pendant group was calculated for CMB (2.15 D) compared to the CDMPC (2.04 D). Thus, π-π and

dipole-dipole interactions as well as HBs with analytes having HB donor properties s are the main interactions which may underlie analyte-selector contact on the CMB [38-40]. Due to their electronic properties, the carbonyl oxygens of the CMB may serve as XB acceptors toward analytes containing halogen atoms with enhanced electrophilic properties. It is worth mentioning that this possible function of the CMB was unexplored so far.

Analytes **1**-**14** feature halogen atoms (**1**-**3** and **7**-**14**), methyl (**4**) and aromatic (**5**,**6**) groups as substituents of 1,2- and 1,3-disubstituted ferrocene scaffolds. The recognition site pattern of these compounds was explored by *V* analysis (Supporting Information, Tables S3 and S4) [4,5]. The local electron charge density of specific molecular regions of the analytes was determined in terms of positive and negative V_S which, in turn, may be associated with electrophilic and nucleophilic sites, respectively. The triple bond π-cloud may function as HB acceptor with the CDMPC, but not with the CMB. Moreover, the presence of the triple bond contributes to better define the stereochemical differences between the enantiomers of compounds **1**-**9** compared to compounds **10**-**12** and **13**-**14**. As a consequence, in the latter series the steric similarity of the halogen substituents may limit the differentiation of the two enantiomers (Table S3). In particular, compounds **5** (R = Ph) and **6** (R = 2-naphthyl) present extended π-electronic clouds involving the triple bond, the cyclopentadienyl ring, and the aromatic substituent. This type of electronic structure may be prone to exert π-π interactions, and also offers better possibility for filling hydrophobic cavities compared to flat aryl and heteroaryl rings. All halogen atoms featuring compounds **1**-**14** show electrophilic σ-hole regions on the elongation of the C-X (X = Cl, Br, I) which, in principle, may participate in XBs as XB donors (I > Br > Cl) with the carbonyl oxygens of the CSPs functioning as XB acceptors. In this regard, it is worth mentioning that the triple bond, exerting an electron-withdrawing effect on the iodine, activates the halogen as electrophile. Consequently the $V_{s,max}$ associated to the iodine is more positive for compounds **1**-**9** compared to compounds **10**-**14**. Moreover, halogens may serve *a)* as HB and XB acceptors (I < Br < Cl < F) through the region of higher electron density, which forms a belt orthogonal to the C–X covalent bond, b) as hydrophobic centres (I > Br > Cl > F), and *c)* as bulky groups participating in repulsive interactions, in particular the heavy halogens such as bromine and iodine.

Thus, in principle, several types of noncovalent interactions may occur between selector and selectand. In this frame, MP polarity has a pivotal role to finely modulate analyte-selector interaction through selective solvent-adsorption phenomena and by participating in the solvation shells of all the interacting partners. In addition, the solvent components of the MP can impact the overall structure and size of the chiral grooves within the polymeric network. On this basis, the effect of MP on the enantioseparations was evaluated under multimodal elution conditions.

3.1 Chromatographic screening

Three chromatographic systems generated by the combination of the Lux Cellulose-3 with *n*-hexane/2-PrOH 95:5 v/v, pure MeOH, and MeOH/water 90:10 v/v as MPs, were evaluated and characterized by *k* (Supporting Information, Figs. S1 and S2) and α values (Fig. 3) toward ferrocenes **1**-**14**. The chromatographic results obtained at 25 °C were compared with the enantioseparation outcomes previously reported for this family of chiral ferrocenes with Lux Cellulose-1, under the same elution conditions [4,5] (Supporting Information, Tables S5-S18). Whereas only **3**, **4**, and **5** could be enantioseparated on Lux Cellulose-1 with $1.14 \leq \alpha \leq 1.51$, baseline enantioseparations were obtained for compounds **2**-**9** on Lux Cellulose-3, with α values ranging from 1.27 to 1.77. In particular, compounds **2**-**4** (R = Cl, Br, and Me, respectively), **7** (R = F) and **8** (R = Cl) could be enantioseparated by using all three elution modes, **6** (R = 2-naphthyl) and **9** (R = Br) with MeOH and aqueous MeOH, whereas ferrocene **5** (R = Ph) under normal phase conditions exclusively. The highest baseline enantioseparation was obtained for ferrocene **3** (R = Br) with MeOH/water 90:10 v/v (α = 1.77). Otherwise, compounds **1** (R = F) and **11**-**14** were only partially separated, and compound **10** (R = F) was not separated under all elution conditions. Evaluating the impact of the elution mode on the enantioseparations, selectivity factors increased following the order *n*-hexane/2-PrOH ≤ MeOH < MeOH/water for ferrocenes **1**-**4**, **6**-**9**, and **11**-**14**, whereas only ferrocene **5** (R = Ph) showed the opposite trend. Retention of the first eluted enantiomer increased following the order *a)* MeOH < *n*-hexane/2-PrOH < MeOH/water for ferrocenes **4**-**6** and **8**-**13**, *b)* MeOH < MeOH/water < *n*-hexane/2-PrOH for **1**-**3** and **7**, and *c)* *n*-hexane/2-PrOH < MeOH < MeOH/water for **14**. Interestingly, the impact of MP on retention of the second eluted enantiomer followed the same trend in all cases with the exception of derivative **5** (R = Ph) (MeOH < MeOH/water < *n*-hexane/2-PrOH). The peculiarity of ferrocene **5** concerning the

impact of MP on retention and selectivity disclosed the presence of a distinctive mechanism underlying binding and enantioselective recognition of this analyte on the CMB. As confirmation of this hypothesis, a reversal of EEO by changing **5** (*R*-*S*) to the structurally related **6** (*S*-*R*) as well as an opposite behaviour of the two compounds by changing the MP from *n*-hexane/2-PrOH (α (**5**) > α (**6**)) to MeOH/water 90:10 (α (**5**) < α (**6**)) could be observed (Supporting Information, Fig. S5). This trend may suggest that the Ph substituent of **5** participates more efficiently in π-π interactions than the larger 2-naphthyl substituent (**6**) which is more prone to fill the hydrophobic cavity of the CSP with MeOH-containing MPs. On the other hand, for ferrocenes **4**-**6**, the impact of the substituent on the enantioseparation depended on the elution mode. Thus, whereas under normal phase conditions selectivity factors increased following the order 2-naphthyl < Me < Ph, a different trend could be observed with MeOH and aqueous MeOH (Ph < 2-naphthyl < Me).

Given that temperature may impact enantioseparation, it was considered as a variable to optimize the separation [41-43], and the dependence of the enantioseparation on the temperature was also explored. On this basis, baseline enantioseparations could also be achieved for compound **9** with the mixture *n*-hexane/2-PrOH 95:5 v/v at 5 °C ($\alpha_{25°C}$ = 1.16 → $\alpha_{5°C}$ = 1.21). With MeOH/water 90:10 v/v, baseline enantioseparation was obtained for compounds **1** ($\alpha_{25°C}$ = 1.17 → $\alpha_{5°C}$ = 1.24) and **5** ($\alpha_{25°C}$ = 1.08 → $\alpha_{5°C}$ = 1.26) at 5 and 10°C, respectively. Enantioseparation was also improved for **13** under normal phase at 5°C. Nevertheless, baseline enantioseparation was not obtained in this case.

Concerning the impact of analyte structures on the enantioseparation with the Lux Cellulose-3, as expected the enantioseparability of dihalogenated derivatives **10**-**14** was in general lower compared to the iodoethynyl substituted derivatives **1**-**9**. It is worth mentioning that for compounds **10**-**14** the use of other MPs such as *n*-hexane/2-PrOH/MeOH, *n*-hexane/ethanol, *n*-hexane/ethanol/MeOH with various concentrations of alcoholic additives, ACN, aqueous ACN and MeOH/water 80:20 did not allow for improving their enantioseparation (chromatographic data are not reported). As mentioned above, steric and electronic factors could explain this trend that was also observed by using the Lux Cellulose-1 as chiral column (Fig. 3). Retention of the first and the second eluted enantiomers was also higher for compounds **1**-**9** compared to the series **10**-**14** (Supporting Information, Figs. S1 and S2). Concerning the impact of

the substitution pattern (1,2 vs 1,3), halogen dependent trends were observed for compounds **1**-**9**. Indeed, 1,2-disubstituted ferrocene **1** showed selectivity factors (1.10 ≤ $\alpha_{25°C}$ ≤ 1.17) lower than those of 1,3-disubstituted compound **7** (1.44 ≤ $\alpha_{25°C}$ ≤ 1.50), both compounds featuring R = F as substituent. Otherwise, the opposite trend was observed for R = Cl, Br, so that compounds **8** and **9** showed lower selectivity factors compared to ferrocenes **2** and **3**. These results could be reasonably due to the balance between two different effects: *a)* in the series **7**-**9** the substituents are sterically more available to interact with the selector, whereas in the **1**-**3** series intramolecular contact between the electronic clouds of close substituents may reduce their availability for intermolecular interactions; *b)* for the larger ferrocenes **7**-**9**, the impact of halogen size (Cl and Br) may be detrimental for the enantioselective recognition in the chiral cavities of the CMB. As a result, evaluating the impact of the substituents for the halogenated series **1**-**3** and **7**-**9**, selectivity factors increased following opposite orders, F < Cl < Br and Br < Cl < F, respectively, under all elution modes.

A different trend was observed for the small compounds **10** / **13** (R = F) and **11** / **14** (R = Cl), and in both cases the 1,2-disubstituted derivatives provided lower α compared to the 1,3-disubstituted series.

The EEO was *R*-*S* in almost all cases for compounds **1**-**6** and **9**, the elution sequence being *S*-*R* only for **4** and **6**. Actually, for **4** the EEO reversal is not substantial but rather due to a change of group priority on the basis of the Cahn-Ingold-Prelog rules. No solvent-dependent EEO reversal was observed.

3.2 Comparison of Lux Cellulose-3 and Lux Cellulose-1

For the enantioseparation of compounds **1**-**14**, Lux Cellulose-3 showed to be superior compared to Lux Cellulose-1 in almost all cases (Fig. 3). Among the 42 enantioseparations considered in this study (14 analytes x 3 elution modes), Lux Cellulose-1 showed better selectivity only in six cases, for compounds **4** and **10**-**12** under normal phase elution conditions, and for **5** and **11** with aqueous MeOH. The impact of solvent was very different for the two chiral columns. In particular, whereas the use of MeOH, as a MP, had a beneficial effect on enantioseparation with Lux Cellulose-3, this solvent was detrimental for the enantioseparation with Lux Cellulose-1, and a drop of selectivity could be observed in this case for almost all compounds. In some cases, the halogen substituent of compounds **1**-**3** and **7**-**9** differently impacted the enantioseparation with the two columns (Supporting Information, Figs. S3 and S4):

a) for compounds **1**-**3**, whereas the enantioselectivity increased following the order F < Cl < Br under normal phase (Fig. S3b) and aqueous MeOH (Fig. S3d) elution conditions on Lux Cellulose-3, and with aqueous MeOH on Lux Cellulose-1 (Fig. S3c), the α values increased following the order Cl < F < Br on the CDMPC-based column with the mixture *n*-hexane/2-PrOH 95:5 v/v (Fig. S3a); *b)* for compounds **7**-**9**, the enantioselectivity increased following the order Br < Cl < F under normal phase (Fig. S4b) and aqueous MeOH (Fig. S4d) elution conditions on Lux Cellulose-3. Otherwise, on Lux Cellulose-1 separation factors increased following the orders F < Cl < Br (Fig. S4a) and F,Br < Cl (Fig. S4c) with the mixture *n*-hexane/2-PrOH 95:5 v/v and aqueous MeOH, respectively. These different halogen dependent trends may derive from the interplay of different factors: *a)* the size of the halogen (F < Cl <Br); *b)* the double function of the halogens on the CDMPC-based column, as HB acceptors toward the N-H of the carbamates, and as XB donors toward the O=C; *c)* the function of halogens as XB donors on the CMB-based column.

Numerous cases of pendant group-dependent EEO reversal were observed (Tables S5-S18, supporting information): *a)* for **3**-**5** and **9** under normal phase conditions; *b)* for **2**-**6**, and **8** with aqueous MeOH; *c)* for **6** with MeOH. It is interesting to note that for **6**, EEO reversal was observed for methanol-containing MP but not under normal phase conditions, the EEO being *S*-*R* on both columns in this elution mode. As a consequence, MP-dependent EEO reversal could be observed for **6** on the Lux Cellulose-1 by changing *n*-hexane/2-PrOH mixture (EEO = *S*-*R*) to aqueous MeOH (EEO = *R*-*S*), but not with Lux Cellulose-3. This result could confirm the hydrophobic nature of the recognition mechanism of **6** on the CMB also under normal phase elution conditions. Moreover, it is worth noting that EEO reversals dependent on pendant group occurred for compounds **1**-**9** exclusively. Considering that on the CDMPC the amidic hydrogen of the carbamate could behave as HB donor toward the triple bond π-cloud and the electron-rich belt of the halogens, it could be hypothesized that the lack of this site in the CMB could contribute to change the enantioselective mechanism compared to the CDMPC.

Interestingly, whereas the Lux Cellulose-3 is superior to Lux Cellulose-1 for the enantioseparation of all halogenated compounds **1**-**3** and **7**-**9** (Supporting Information, Figs. S3 and S4), the two columns exhibited a certain degree of complementarity

towards compounds **4**-**6** under both normal phase and aqueous methanol elution conditions (Fig. S5).

3.3 Effect of temperature on enantioseparation

The van't Hoff equations (see Supporting Information for details) allow for determining the macroscopic thermodynamic quantities governing enantiomer adsorption and enantioseparation [41-44]. Although the molar quantities determined on the basis of van't Hoff equations are, as a matter of fact, composite values representing non-enantioselective sites (type I) and enantioselective sites (type II) [45-47], interesting information on analyte/CSP association can be obtained on the basis of thermodynamic considerations by applying van't Hoff analysis [41-44]. In addition, given that thermodynamic parameters are depending on analyte, CSP and MP, useful information can be gained by comparison of thermodynamic data as subtle variations of the chromatographic system (analyte, CSP, MP) occur.

Thus, with the aim to compare the thermodynamic profiles of the CMB- and CDMPC-based chiral columns, retention and selectivity of compounds **1**-**9** on Lux Cellulose-3 were determined at different temperatures from 5 to 40 °C, in 5 °C increments, by using *n*-hexane/2-PrOH 95:5 v/v (Supporting Information, Figures S6-S13) and MeOH/water 90:10 v/v (Figures S16-S24) as MPs. For compounds **1**-**3** and **7**-**9** the thermodynamics parameters, determined with Lux Cellulose-1 under the same elution conditions and recently reported, were used as reference for comparison [5]. For compounds **4** and **5**, the thermodynamic profiles on Lux Cellulose-1 were derived in the frame of the present study (Figures S14, S15, and S25-S27). The results of the analyses at variable temperature of ferrocene **6** on the Lux Cellulose-3 under normal phase provided an unusual thermodynamic profile. However, these data are not reported and discussed herein because this issue requires further investigations before publication.

The thermodynamic parameters, enthalpy ($\Delta\Delta H°$), entropy ($\Delta\Delta S°$) and free energy ($\Delta\Delta G°$) differences, isoenantioselective temperatures (T_{iso}) and thermodynamic (enthalpy/entropy) ratios (Q), are reported in Tables 1 and 2 as derived from van't Hoff analysis. The entropy-enthalpy compensation graphs for the four chromatographic systems Lux Cellulose-3/*n*-hexane/2-PrOH 95:5 v/v (A), Lux Cellulose-1/*n*-hexane/2-PrOH 95:5 v/v (B), Lux Cellulose-3/MeOH/water 90:10 v/v (C), and Lux Cellulose-

1/MeOH/water 90:10 (D) with compounds **1**-**9** are reported in Figure 4. On this basis, the following remarks can be made:

a) for compounds **1**-**9**, the enantioseparations were enthalpy-driven on the CMB in almost all cases (Fig. 4A) because the temperature range was below the calculated T_{iso}, and the thermodynamic ratio $Q = \Delta\Delta H / (298 \times \Delta\Delta S) > 1$ under normal phase elution conditions (Table 1) and with aqueous MeOH (Table 2). In a previous study performed by using CDMPC, compounds **1** and **2** under normal phase had shown entropy-driven and mixed enthalpy/entropy-driven thermodynamic profiles (Fig. 4B);

b) in general, the contribution of the enthalpy component to the free energy difference was higher for Lux Cellulose-3 compared to the Lux Cellulose-1 with both MPs;

c) by comparing the thermodynamic profiles of **1** (R = F) and **3** (R = Br) on CMB under normal phase, it could be observed that the enantioseparation increased as the enthalpy contribution to free energy difference decreased. Otherwise, with MeOH/water 90:10 the opposite occurred and decreasing the enthalpy contribution to free energy difference appeared to be detrimental for the enantioseparation of compounds **1** and **3**;

d) interestingly, a different trend was observed for **2** bearing chlorine substituent with intermediate electronic properties compared to **1** and **3**. Indeed, ferrocene **2** presented the lowest enthalpy contribution to free energy differences within the series **1**-**3**, but intermediate α values compared to **1** and **3** with both elution mode;

e) analogously, for the same series **1**-**3** the increase of selectivity factors observed by changing *n*-hexane/2-PrOH to MeOH/water as MPs corresponded to different trends in terms of entropy/enthalpy ratio. Indeed, whereas for **2** the *Q* values increased as 1.60 → 1.90 by changing the *n*-hexane mixture to that containing MeOH, for **1** and **3** *Q* decreased as 2.61 → 1.91 and 2.14 → 1.98, respectively;

f) for the enantioseparation of compounds **7**-**9** on CMB under normal phase, increasing the enthalpy contribution to free energy difference in the order F < Cl < Br appeared to be detrimental for the enantioseparation which decreased following the order F > Cl > Br. Otherwise, with MeOH/water 90:10 the opposite occurred and decreasing the enthalpy contribution to free energy difference in the order F > Cl > Br appeared to be detrimental for the enantioseparation.

Thus, the enantioseparation could be optimized by tuning the MP (elution mode) which, in turn, determined the noncovalent interaction pattern and, consequently, the thermodynamic profile of the recognition pathway.

3.4 Molecular dynamics simulations

MD simulations were performed with the aim *a)* to confirm that XB actually participates in the enantioselective recognition, and *b)* to explore the noncovalent interaction pattern of CMB and CDMPC for a given analyte as test probe. It is worth mentioning that in our previous study, the possibility of XB-driven enantioseparation was reasonably demonstrated for iodoethynyl ferrocene **3** on CDMPC through *V* and related source function decomposition theoretical analyses [5]. Thus, the enantioseparations of **3** on the two CSPs, with *n*-hexane/2-PrOH 95:5 v/v as MP, were considered and modelled as benchmark experimental data. These enantioseparations appeared suitable for this purpose given that different separation factors (Supporting Information, Table S7), EEO, and thermodynamic parameters (Table 1) were obtained for **3** on the two CSPs.

The theoretical investigation based on MD simulations was performed by using CMB and CDMPC nonamers as virtual models of the polysaccharide-based selectors. The 100 ns MD simulations in the AMBER force field [48] were performed by using the mixture *n*-hexane/2-PrOH 95:5 as explicit virtual solvent in accord with the experimental conditions used in the chromatographic analyses. With the aim to confirm the hypothesis that a XB involving the halogen substituents of ferrocene **3** participates in selector-selectand complex formation, the explicit σ-hole (ESH) parametrization [49,50] was used to model the electrophilic electron charge density depletion on the halogen atoms [51] (see Supporting Information for details). For both (*R*)- and (*S*)-**3**, the simulations were performed by using three virtual electronic conditions: *a)* without ESH parametrization, virtually suppressing the electrophilic feature of the halogens; *b)* introducing the ESH parametrization on the bromine atom, exclusively. This choice was justified by the fact that the enantioseparation outcomes within the series **1**-**3** appeared to be related to the nature of the halogen (F, Cl, Br, respectively). Indeed, the stereoelectronic properties of the iodine were substantially the same in the three compounds (Supporting Information, Table S3), thus iodine could not be the origin of the different enantioselective recognition observed for each member of the series [5]; *c)* introducing the ESH parametrization on both bromine and

iodine in order to see if energy differences occurred compared to simulations performed under conditions *b)*.

As a result, in the case *a)*, *S*-*R* was obtained as virtual EEO for the enantioseparation of **3** on CMB. Thus, suppressing the electrophilic feature of the halogens provided the wrong EEO and, consequently, a virtual model not consistent with the real experiment (EEO_{exp} = *R*-*S*). Under the conditions *c)*, the simulations provided the same results as in the case *b)*. This result confirmed that the iodine was not critical for the enantioselective recognition. On this basis, only the simulations obtained under conditions *b)* will be discussed in details herein.

The total interaction energies calculated for (*R*)- and (*S*)-**3** in their complexes with each of the polysaccharide nonamers are summarized in Table 3. The reported energies are mean values that were calculated from 5000 complexes obtained by snapshots taken every 20 ps from the 100 ns MD trajectories. The interaction energy (E_{int}) between enantiomer and selector was calculated on the basis of the energies of the selector-enantiomer complex, the selector, and the enantiomer (Eq. 1)

$$E_{int} = E_{total} - E_{enantiomer} - E_{polysaccharide-based\ selector} \quad (1)$$

where the E_{int} term is derived from the contributions of the van der Waals (vdW) and the electrostatic (el) interaction terms (Eq. 2).

$$E_{int} = E_{el} + E_{vdW} \quad (2)$$

In Fig. 5, representative snapshots and noncovalent interactions from the simulated MD trajectories of the (*R*)- and (*S*)-**3** complexes with CDMPC (A,B) and CMB (C,D) are depicted. The following remarks can be made:

a) a more compact hydrophobic cavity was observed for CMB (C,D) compared to CDMPC (A,B);

b) the calculated EEOs (Table 3) were fully consistent with the experimental elution sequence;

c) the E_{int} values of the (*R*)- and (*S*)-**3** on CDMPC and CMB were fully consistent with retention times following the order $(S)_{CDMPC}$-**3** (8.93 min) < $(R)_{CDMPC}$-**3** (9.78 min) < $(R)_{CMB}$-**3** (10.26 min) < $(S)_{CMB}$-**3** (12.89 min);

d) different noncovalent interaction patterns were observed with the two CSPs: *i)* in the (*S*)-**3**/CDMPC complex a Br···O=C interaction and a π-π interaction involving the triple bond π-cloud and the 3,5-dimethylphenyl of the CDMPC (Fig. 5A); *ii)* in the (*R*)-

3/CDMPC complex a Br···O=C interaction and a HB between the amidic hydrogen of the selector and the electron rich belt of the bromine (Fig. 5B); *iii)* shorter Br···O=C interactions could be observed for both (*R*)-**3**/CMB (Fig. 5C), and (*S*)-**3**/CMB (Fig. 5D) complexes. It is worth mentioning that for the CMB-complexes, shorter distances and angle values closer to the reference value of 180° indicated the presence of stronger XBs;

e) this observation could be consistent with the higher enthalpic contribution to the free energy difference determined by the thermodynamic analysis for CMB (Q = 2.14) compared to the CDMPC (Q = 1.15). In addition, the different strength of the XBs in CDMPC and CMB could be also consistent with the higher electron charge density on the carbonyl oxygen calculated for the CMB compared to the CDMPC.

4 Concluding remarks

In this study, the enantioseparation of ferrocenes **1**-**14** has been systematically explored under multimodal elution conditions by using the cellulose 4-methylbenzoate-based Lux Cellulose-3 as chiral column. As a result, methods for baseline enantioseparations were successfully developed for nine compounds (**1**-**9**) with selectivity factors ranging from 1.24 to 1.77. In particular, compounds **2**, **5** and **7**-**9** could be baseline enantioseparated by using a *n*-hexane-based MP, this elution condition being useful for semipreparative purposes given the possibility to remove the MP at relatively low temperatures. It is worth mentioning that the cellulose carbamate-based Lux Cellulose-1 was unable to enantioseparate these compounds under normal phase elution conditions [5]. Otherwise, 1-halo-2-iodoferrocene **10**-**12** and 1-halo-3-iodoferrocenes **13** and **14** could be only partially enantioseparated on the Lux Cellulose-3, these results confirming that the enantioseparation of nonpolar planar chiral ferrocenes remains rather challenging. On the other hand, in a previous study we found that planar chiral ferrocenes **10**-**14** were also poorly enantioseparated on cellulose carbamate-based CSPs, whereas amylose carbamate-based CSPs were only able to baseline enantioseparate compounds **13** and **14** with MeOH-containing MPs. Due to the hydrophobic feature of the ferrocenes used in this study as analytes, using aqueous MeOH-containing MPs allowed improving enantioseparation performances of the benzoate-based chiral column for ferrocenes **1**-**4**, **6**-**9**, **13** and **14**.

van't Hoff thermodynamic analysis allowed to observe different enthalpy and entropy contributions to the $\Delta\Delta G°$ associated to the enantioseparations strictly dependent on the CSP pendant groups (carbamate or benzoate), MP polarity and the nature of the substituents of the analytes. In particular, it was found that the type and the position of the halogen substituents (F, Cl, Br) may impact the thermodynamic contributions to $\Delta\Delta G°$. The thermodynamic analysis also confirmed that the elution mode may significantly determine the thermodynamic profile of the recognition as a result of the modulation of the noncovalent interactions underlying selector-selectand complex formation.

Finally, MD simulations of the enantioseparation of the iodoethynyl ferrocene **3** were performed exploring the molecular bases of the enantioselective recognition of this chiral compound, used as test probe on CDMPC and CMB. The theoretical analyses disclosed that actually XBs can participate in the recognition mechanism of halogenated ferrocenes on cellulose-based selectors with efficacy dependent *a)* on the properties of the selector as XB acceptor and *b)* on the presence of competitive noncovalent interactions which may oppose to or weaken XBs. It is worth mentioning that these simulations represent the first attempt to model enantioseparation of planar chiral ferrocenes on cellulose-based selectors.

Acknowledgements

We thank CNR (Consiglio Nazionale delle Ricerche) (grant SAC.AD002.011.025) and SRNSFG (Shota Rustaveli National Science Foundation of Georgia) (grant CNR-19-075) for the Joint Bilateral Agreement, the University of Strasbourg, the Centre National de la Recherche Scientifique (CNRS), and French National Research Agency (ANR-21-CE07-0014) for financial support.

Conflict of interest

The authors have declared no conflict of interest.

Data availability statement

The data that support the findings of this study are available from the corresponding author upon reasonable request.

5 References

[1] Schlögl KA, Widhalm M. Recycling technique for the chromatographic separation of enantiomers and diastereomers on triacetylcellulose. Monatsh Chem. 1984;115:1113–20.

[2] Yamazaki Y, Uebayasi M, Hosono K. Enantiotopic differentiation in horse-liver alcohol-dehydrogenase-catalyzed oxidoreduction studied with novel substrates having organometallic moieties. Eur J Biochem. 1989;184:671–80.

[3] Mayr B, Schottenberger H, Elsner O, Buchmeiser MR. Separation of planar chiral ferrocene derivatives on β-cyclodextrin-based polymer supports prepared via ring-opening metathesis graft-polymerization. J Chromatogr A. 2002;973:115–22.

[4] Dessì A, Sechi B, Dallocchio R, Chankvetadze B, Pérez-Baeza M, Cossu S, et al., Comparative enantioseparation of planar chiral ferrocenes on polysaccharide- based chiral stationary phases. Chirality. 2022;34:609–19.

[5] Sechi B, Dessì A, Gatti C, Dallocchio R, Chankvetadze B, Cossu S, et al., Unravelling functions of halogen substituents in the enantioseparation of halogenated planar chiral ferrocenes on polysaccharide-based chiral stationary phases: experimental and electrostatic potential analyses. J Chromatogr A. 2022;1673:463097.

[6] Cantatore C, Korb M, Lang H, Cirilli R. ON/OFF receptor-like enantioseparation of planar chiral 1, 2-ferrocenes on an amylose-based chiral stationary phase: The role played by 2-propanol. Anal Chim Acta. 2022;1211:339880.

[7] Morvan A, Garnier C, Furman C, Speybrouck D, Boulanger E, Ghinet A, et al., Separation of planar chiral ferrocenes by capillary electrokinetic chromatography and liquid chromatography. J Chromatogr A. 2022;1677:463306.

[8] Bonin L, Morvan A, Coadou G, Furman C, Boulanger E, Ghinet A, et al. Supercritical fluid chromatography for separation of chiral planar metallocenes. J Chromatogr A. 2022;1674:463115.

[9] Cunningham L, Benson A, Guiry PJ. Recent developments in the synthesis and applications of chiral ferrocene ligands and organocatalysts in asymmetric catalysis. Org Biomol Chem. 2020;18:9329–70.

[10] Singh A, Lumb I, Mehra V, Kumar V. Ferrocene-appended pharmacophores: An exciting approach for modulating the biological potential of organic scaffolds. Dalton Trans. 2019;48:2840-60.

[11] Urbano A, Del Hoyo AM, Martinez-Carríon A, Carreño MC. Asymmetric synthesis and chiroptical properties of enantiopure helical ferrocenes. Org Lett. 2019;21:4623–7.

[12] Grecchi S, Arnaboldi S, Korb M, Cirilli R, Araneo S, Guglielmi V, et al., Widening the scope of “inherently chiral” electrodes: Enantiodiscrimination of chiral electroactive probes with planar stereogenicity. ChemElectroChem. 2020;7:3429–38.

[13] Peluso P, Mamane V. Ferrocene derivatives with planar chirality and their enantioseparation by liquid-phase techniques. Electrophoresis. 2022; DOI: 10.1002/elps.202200148

[14] Butenschön H. Haloferrocenes: syntheses and selected reactions. Synthesis. 2018;50:3787–808.

[15] Tazi M, Hedidi M, Erb W, Halauko YS, Ivashkevich OA, Matulis VE, et al., Fluoro- and chloroferrocene: from 2- to 3-substituted derivatives. Organometallics. 2018;37:2207–21.

[16] Mamane V, Peluso P, Aubert E, Weiss R, Wenger E, Cossu S, et al., Disubstituted ferrocenyl iodo- and chalcogenoalkynes as chiral halogen and chalcogen bond donors. Organometallics. 2020;39:3936–50.

[17] Rios R, Liang J, Lo MM-C, Fu GC. Synthesis, resolution and crystallographic characterization of a new C_2-symmetric planar-chiral bipyridine ligand: application to the catalytic enantioselective cyclopropanation of olefins. Chem Commun. 2000;377–8.

[18] Tsukazaki M, Tinkl M, Roglans A, Chapell BJ, Taylor NJ, Snieckus V. Direct and highly enantioselective synthesis of ferrocenes with planar chirality by (−)-sparteine-mediated lithiation. J Am Chem Soc. 1996;118:685–6.

[19] Patti A, Pedotti S, Sanfilippo C. Comparative HPLC enantioseparation of ferrocenylalcohols on two cellulose- based chiral stationary phases. Chirality. 2007;19:344–51.

[20] Gao D-W, Zheng C, Gu Q, You S-L. Pd-catalyzed highly enantioselective synthesis of planar chiral ferrocenylpyridine derivatives. Organometallics. 2015;34:4618–25.

[21] Okamoto Y, Kawashima M, Yamamoto K, Hatada K. Useful chiral packing materials for high-performance liquid chromatographic resolution. Cellulose triacetate and tribenzoate coated on macroporous silica gel. Chem Lett. 1984;13:739−42.

[22] Ichida A, Shibata T, Okamoto I, Yuki Y, Namikoshi H, Toda Y. Resolution of enantiomers by HPLC on cellulose derivatives. Chromatographia. 1984;19:280−4.

[23] Okamoto Y, Aburatani R, Hatada K. Chromatographic chiral resolution. XIV. Cellulose tribenzoate derivatives as chiral stationary phases for high-performance liquid chromatography. J Chromatogr A. 1987;389:95−102.

[24] Okamoto Y, Yashima E. Derivatives for chromatographic separation of enantiomers. Angew Chem Int Ed. 1998;37:1020–43.

[25] Chankvetadze B. Recent developments on polysaccharide-based chiral stationary phases for liquid-phase separation of enantiomers. J Chromatogr A. 2012;1269:26–51.

[26] Peluso P, Cossu S. Comparative HPLC enantioseparation of thirty-six aromatic compounds on four columns of the Lux® series. Impact of substituents, shapes and electronic properties. Chirality. 2013;25:709–18.

[27] Peluso P, Chankvetadze B. The molecular bases of chiral recognition in 2-(benzylsulfinyl)benzamide enantioseparation. Anal Chim Acta. 2021;1141:194–205.

630 [28] Peluso P, Dessì A, Dallocchio R, Mamane V, Cossu S. Recent studies of docking
631 and molecular dynamics simulation for liquid-phase enantioseparations.
632 Electrophoresis. 2019;40:1881–96
633 [29] Dallocchio R, Sechi B, Dessì A, Chankvetadze B, Cossu S, Mamane V, et al.,
634 Enantioseparations of polyhalogenated 4,4'-bipyridines on polysaccharide-
635 based chiral stationary phases and molecular dynamics simulations of selector–
636 selectand interactions. Electrophoresis. 2021;42:1853–63.
637 [30] Dayaker G, Sreeshailam A, Chevallier F, Roisnel T, Krishna PR, Mongin F.
638 Deprotonative metallation of ferrocenes using mixed lithium-zinc and lithium-
639 cadmium combinations. Chem Commun. 2010;46(16):2862–4.
640 [31] Tazi M, Erb W, Roisnel T, Dorcet V, Mongin F, Low PJ. From ferrocene to
641 fluorine-containing pentasubstituted derivatives and all points in-between; or,
642 how to increase the available chemical space. Org Biomol Chem. 2019;17:9352–
643 9.
644 [32] Frisch MJ, Trucks GW, Schlegel HB, Scuseria GE, Robb MA, Cheeseman JR,
645 et al., Gaussian 09, Revision B. 01. C.T. Wallingford: Inc. Gaussian; 2010.
646 [33] Lu T, Chen F. Multiwfn: a multifunctional wavefunction analyser. J Comput
647 Chem. 2012;33:580–92.
648 [34] Lu T, Chen F. Quantitative analysis of molecular surface based on improved
649 Marching Tetrahedra algorithm. J Mol Graph Model. 2012;38:314–23.
650 [35] Yamamoto C, Yamada K, Motoya K, Kamiya Y, Kamigaito M, Okamoto Y, et al.,
651 Preparation of HPLC chiral packing materials using cellulose tris(4-
652 methylbenzoate) for the separation of chrysanthemate isomers. J Polym Sci Part
653 A Polym Chem. 2006;44:5087−97.
654 [36] Francotte E, Wolf RM, Lohmann D, Mueller R. Chromatographic resolution of
655 racemates on chiral stationary phases: I. Influence of the supramolecular
656 structure of cellullose triacetate. J Chromatogr A. 1985;347:25−37.
657 [37] Oguni K, Oda H, Ichida A. Development of chiral stationary phases consisting of
658 polysaccharide derivatives. J Chromatogr A. 1995;694:91−100.
659 [38] O'Brien T, Crocker L, Thompson R, Thompson K, Toma PH, Conlon DA, et al.,
660 Mechanistic aspects of chiral discrimination on modified cellulose. Anal Chem
661 1997;69:1999−2007.

[39] Alcaro S, Bolasco A, Cirilli R, Ferretti R, Fioravanti R, Ortuso, F. Computer-aided molecular design of asymmetric pyrazole derivatives with exceptional enantioselective recognition toward the Chiralcel OJ-H stationary phase. J Chem Inf Model. 2012;52:649−54.

[40] Peluso P, Mamane V, Dallocchio R, Dessì A, Cossu S. Noncovalent interactions in high-performance liquid chromatography enantioseparations on polysaccharide-based chiral selectors. J Chromatogr A. 2020;1623:461202.

[41] Peluso P, Sechi B, Lai G, Dessì A, Dallocchio R, Cossu S, et al., Comparative enantioseparation of chiral 4,4'-bipyridine derivatives on coated and immobilized amylose-based chiral stationary phases. J Chromatogr A. 2020;1625:461303.

[42] Matarashvili I, Kobidze G, Chelidze A, Dolidze G, Beridze N, Jibuti G, et al., The effect of temperature on the separation of enantiomers with coated and covalently immobilized polysaccharide-based chiral stationary phases. J Chromatogr A 2019;1599:172–9.

[43] Ianni F, Pataj Z, Gross H, Sardella R, Natalini B, Lindner W, et al., Direct enantioseparation of underivatized aliphatic 3-hydroxyalkanoic acids with a quinine-based zwitterionic chiral stationary phase. J Chromatogr A. 2014;1363:101–8.

[44] Panella C, Ferretti R, Casulli A, Cirilli R. Temperature and eluent composition effects on enantiomer separation of carvedilol by high-performance liquid chromatography on immobilized amylose-based chiral stationary phases. J Pharm Anal. 2019;9:324–31.

[45] Fornstedt T. Characterization of adsorption processes in analytical liquid-solid chromatography. J Chromatogr A. 2010;1217:792−812.

[46] Asnin LD, Stepanova MV. Van't Hoff analysis in chiral chromatography. J Sep Sci. 2018;41:1319–37.

[47] Sepsey A, Horváth E, Catani M, Felinger A. The correctness of van't Hoff plots in chiral and achiral chromatography. J Chromatogr A. 2020;1611:460594.

[48] Maier JA, Martinez C, Kasavajhala K, Wickstrom L, Hauser KE, Simmerling C. ff14SB: improving the accuracy of protein side chain and backbone parameters from ff99SB. J Chem Theory Comput. 2015;11:3696–713.

[49] Ibrahim MAA. Molecular mechanical perspective on halogen bonding. J Mol Model. 2012;18:4625–38.

[50] Kolář M, Hobza P, Bronowska K. Plugging the explicit σ-holes in molecular docking. Chem Commun. 2013;49:981–3.

[51] Dallocchio R, Dessì A, Solinas M, Arras A, Cossu S, Aubert E, et al., Halogen bond in high-performance liquid chromatography enantioseparations: description, features and modelling. J Chromatogr A. 2018;1563:71–81.

Supporting information

Supporting information file: Additional introductive details; Electrostatic potential extrema of selectors and analytes; additional HPLC data; Thermodynamics details; additional MD simulation data.

FIGURE CAPTIONS

Figure 1. Structures and numbering of planar chiral ferrocenes **1**–**14**.

Figure 2. Graphic representations (Chimera 1.13.1, UCSF, San Francisco, USA) of the shape of CDMPC (A) and CMB (B) chiral cavities as derived from MD simulations (see Supporting Information). Colour legend: blue, nitrogen; red, carbonyl oxygen; green, phenyl ring, tan, all other atoms.

Figure 3. Comparison of selectivity factors (α) of compounds **1**-**14** on CDMPC- (red lines/■) and CMB- (blue line/●) based chiral columns under multimodal elution conditions (A, Hex/2-PrOH 95:5 v/v; B, MeOH 100%; C, MeOH/water 90:10 v/v).

Figure 4. Enthalpy (cal/mol)-entropy ($cal \cdot K^{-1} \cdot mol^{-1}$) compensation for compounds **1**-**9**: A) Lux Cellulose-3, *n*-hexane/2-PrOH 95:5 v/v (the values for compound **6** are not included in the graph); B) Lux Cellulose-1, *n*-hexane/2-PrOH 95:5 v/v (the values for compound **6** are not included in the graph); C) Lux Cellulose-3, MeOH/water 90:10 v/v; D) Lux Cellulose-1, MeOH/water 90:10 v/v (flow rate, 0.8 ml/min; temperature range 278.15-313.15 K).

Figure 5. Representative snapshots and noncovalent interactions from the simulated MD trajectories of the complexes of (*R*)- and (*S*)-**3** with CDMPC (A,B) and CMB (C,D).

TABLE CAPTIONS

Table 1. Thermodynamic parameters calculated from the van't Hoff plots (temperature range 278.15-313.15 K) for the enantioseparation of ferrocenes **1**-**5** and **7-9** on the Lux Cellulose-3 with *n*-hexane/2-PrOH 95:5 v/v as a MP (flow rate, 0.8 ml/min). The thermodynamic parameters calculated for the enantioseparation of ferrocenes **1**-**3** and **7**-**9** [5], **4** and **5** on the Lux Cellulose-1 are reported for comparison

Table 2. Thermodynamic parameters calculated from the van't Hoff plots (temperature range 278.15-313.15 K) for the enantioseparation of ferrocenes **1**-**9** on the Lux Cellulose-3 with MeOH/water 90:10 v/v as a MP (flow rate, 0.8 ml/min). The thermodynamic parameters calculated for the enantioseparation of ferrocenes **1**-**3** and **7**-**9** [5], and **4**-**6** on the Lux Cellulose-1 are reported for comparison

Table 3. Interaction energies (E_{int}) (kcal/mol) and component contributions (E_{el}, E_{vdW}) for the association of (*R*)-**3** and (*S*)-**3** with CDMPC (EEO_{exp} = *S*-*R*) and CMB (EEO_{exp} = *R*-*S*)

737

R	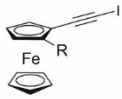	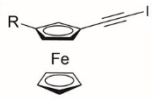		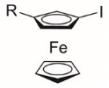
F	1	7	10	13
Cl	2	8	11	14
Br	3	9	12	
Me	4			
Ph	5			
2-Naphth	6			

Figure 1. Structures and numbering of planar chiral ferrocenes **1**–**14**.

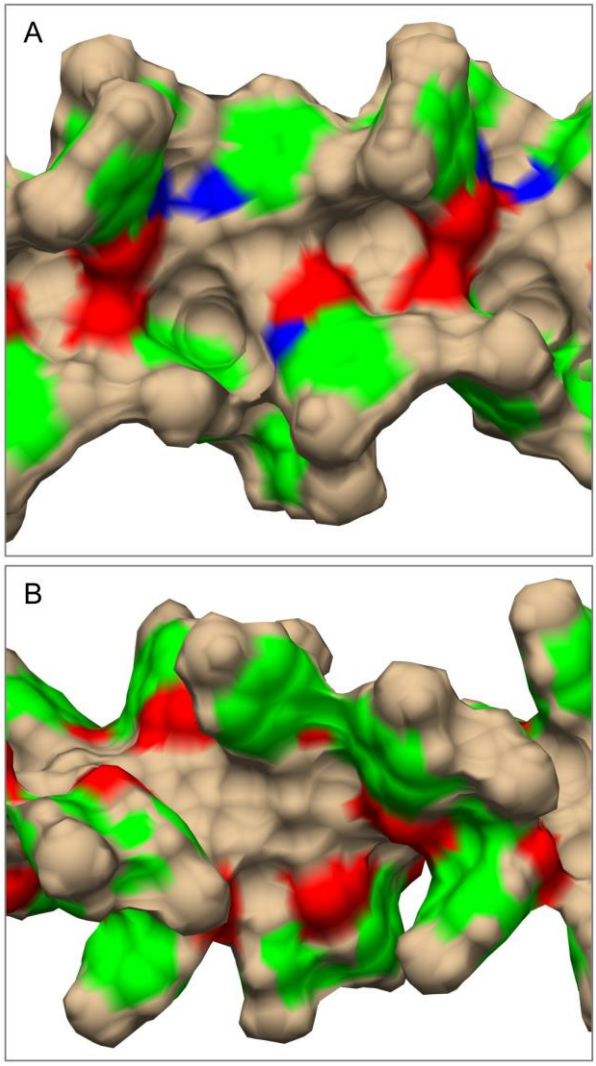

Figure 2. Graphic representations (Chimera 1.13.1, UCSF, San Francisco, USA) of the shape and dimensions of CDMPC (A) and CMB (B,C) chiral cavities as derived from MD simulations (see Supporting Information): surfaces (A, B), only the carbonyl oxygens are coloured in red; tube model (C). Colour legend: blue, nitrogen; red, oxygen; green, phenyl ring.

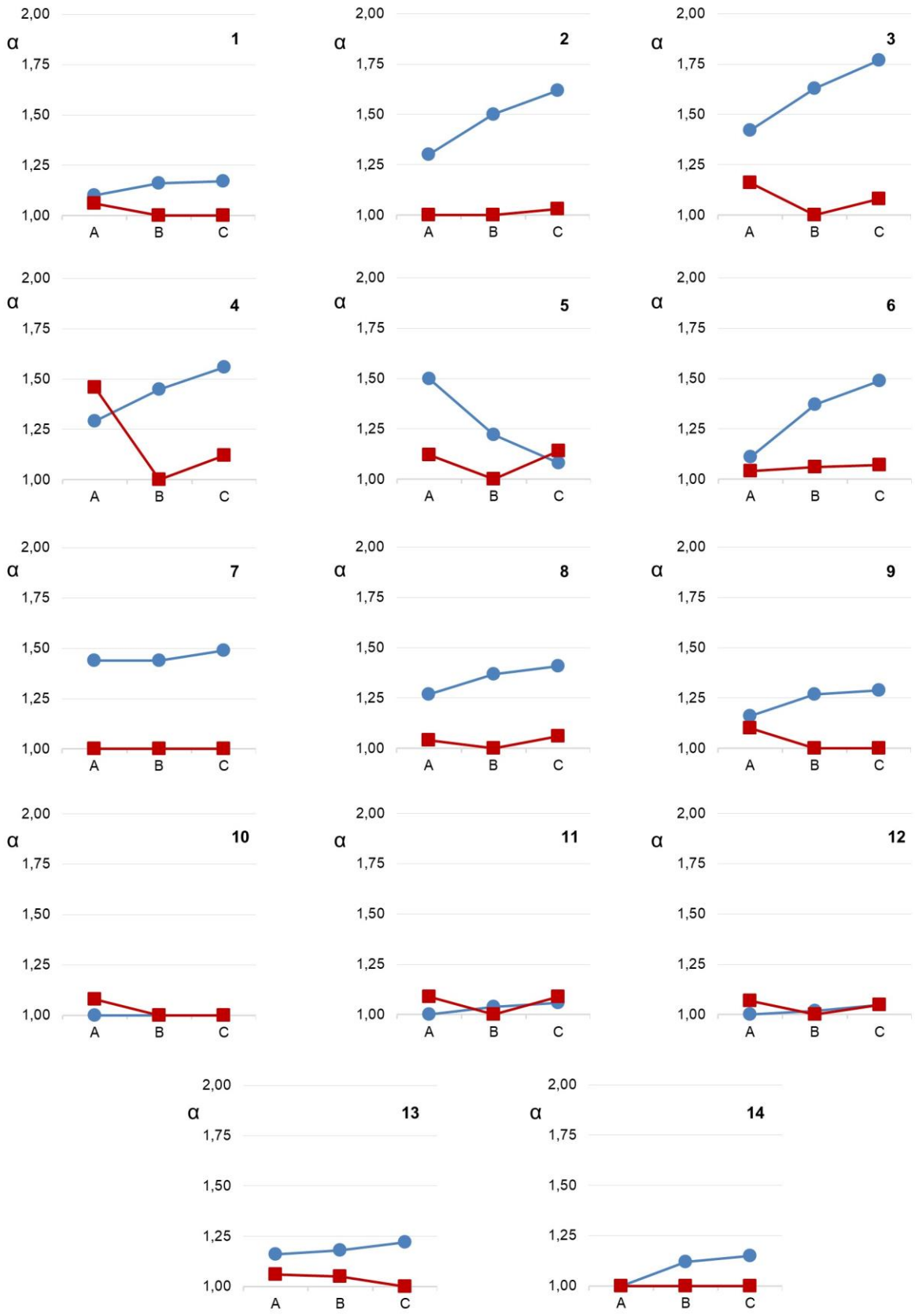

747

748 **Figure 3.** Comparison of selectivity factors (α) of compounds **1**-**14** on CDMPC- (red
749 lines/■) and CMB- (blue line/●) based chiral columns under multimodal elution
750 conditions (A, Hex/2-PrOH 95:5 v/v; B, MeOH 100%; C, MeOH/water 90:10 v/v).

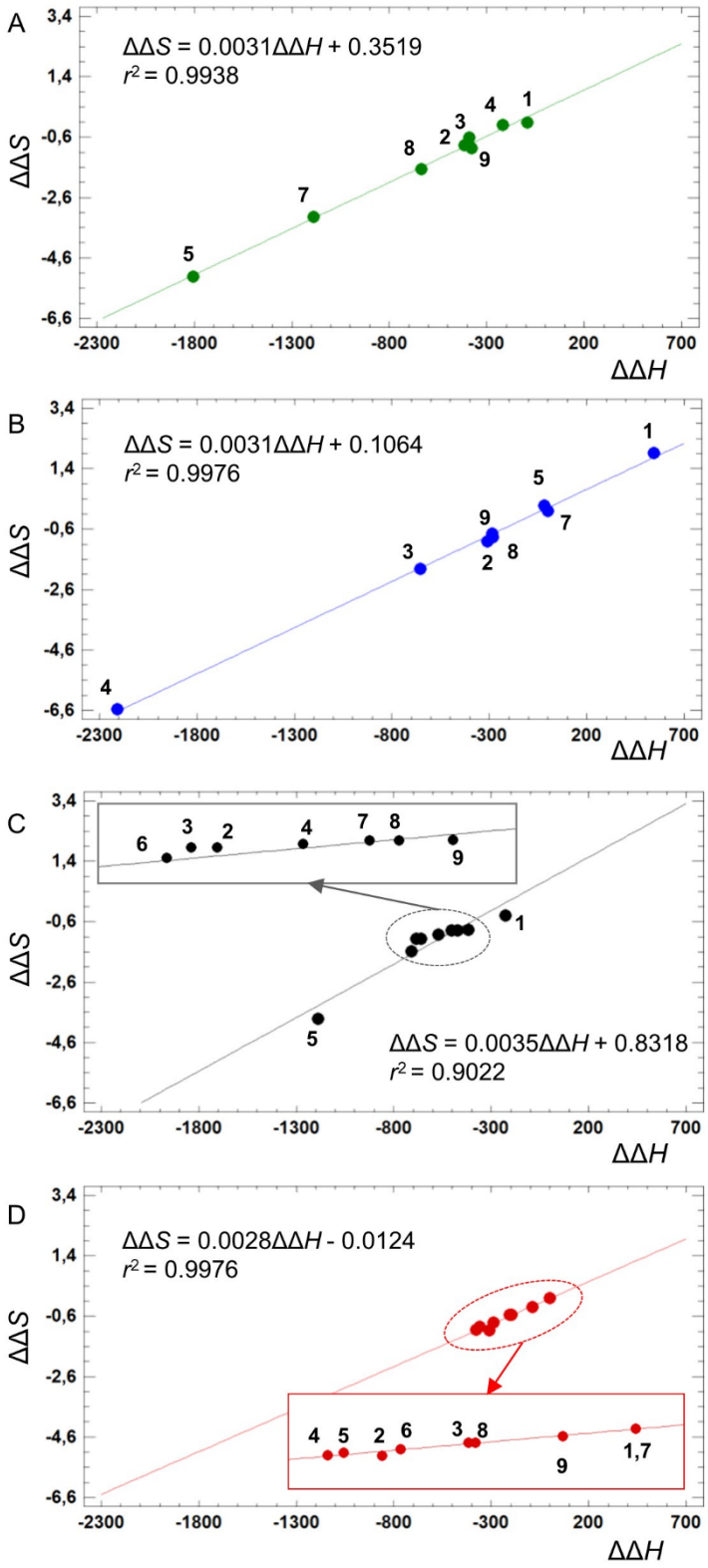

Figure 4. Enthalpy-entropy compensation for compounds **1**-**9**: A) Lux Cellulose-3, *n*-hexane/2-PrOH 95:5 v/v (the values for compound **6** are not included in the graph); B) Lux Cellulose-1, *n*-hexane/2-PrOH 95:5 v/v; C) Lux Cellulose-3, MeOH/water 90:10 v/v; D) Lux Cellulose-1, MeOH/water 90:10 v/v (*FR* 0.8 ml/min, temperature range 278.15-313.15 K).

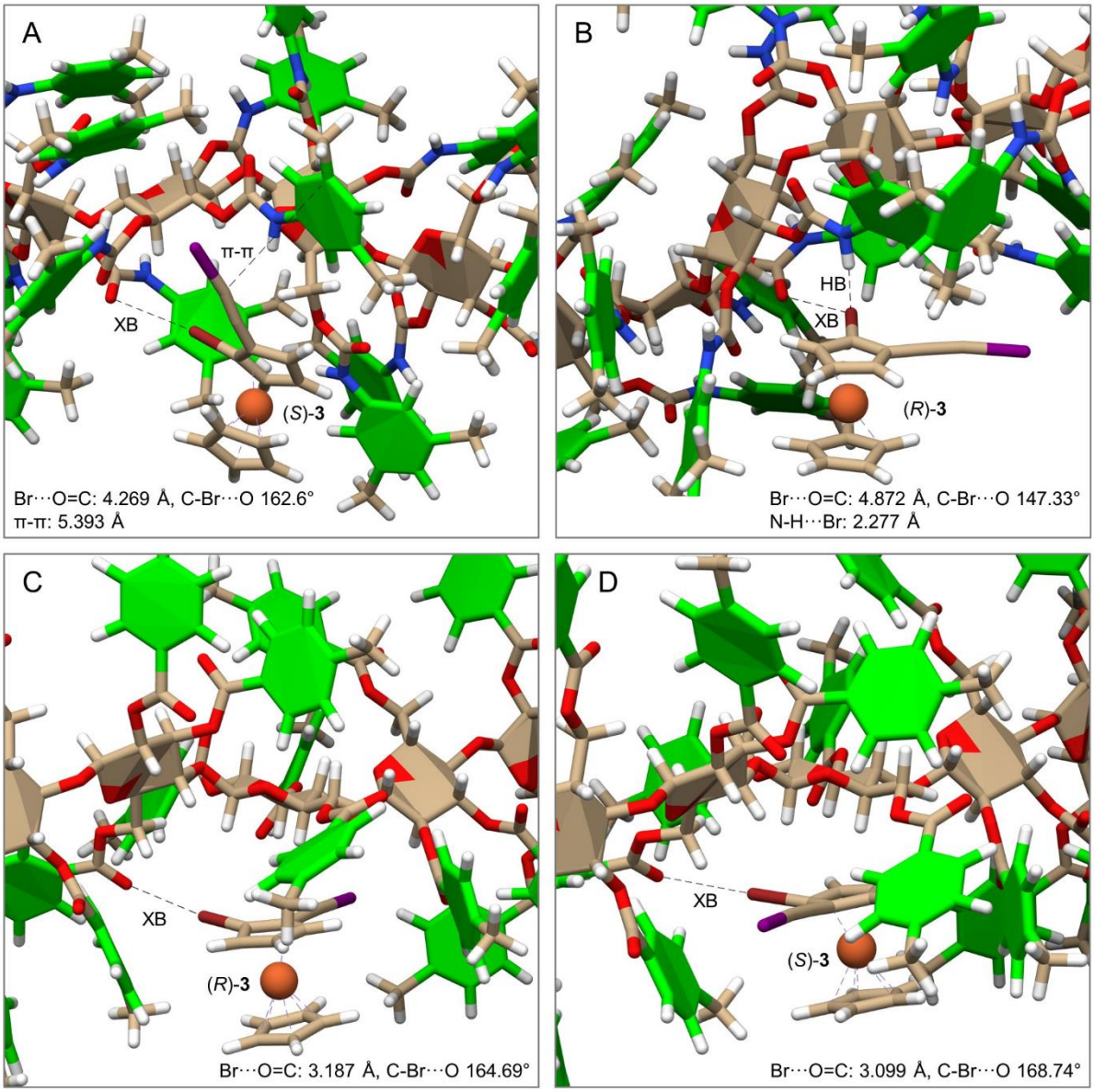

Figure 5. Representative snapshots and noncovalent interactions from the simulated MD trajectories of the complexes of (*R*)- and (*S*)-**3** with CDMPC (A,B) and CMB (C,D). Colour legend: bright red, oxygen; brown, iron; dark red, bromine; green, phenyl ring; tan, carbon; violet, iodine; white, hydrogen.

764 **Table 1.** Thermodynamic parameters calculated from the van't Hoff plots (temperature range
765 278.15-313.15 K) for the enantioseparation of ferrocenes **1**-**5** and **7-9** on the Lux Cellulose-
766 3 with *n*-hexane/2-PrOH 95:5 v/v as a MP (flow rate, 0.8 ml/min). The thermodynamic
767 parameters calculated for the enantioseparation of ferrocenes **1**-**3** and **7**-**9** [5], **4** and **5** on the
768 Lux Cellulose-1 are reported for comparison

Fc	Column	EEO	ΔΔH (cal/mol)	ΔΔS ($cal \cdot K^{-1} \cdot mol^{-1}$)	ΔΔG (cal/mol)	T_{iso}, K (°C)	Q
1	Cellulose-3	*R*-*S*	-93.55	-0.12	-57.77	780 (506)	2.61
	Cellulose-1	*R*-*S*	543.96	1.93	-31.47	282 (7)	0.94
2	Cellulose-3	*R*-*S*	-415.59	-0.87	-156.20	478 (204)	1.60
	Cellulose-1	*S*-*R*	-311.64	-1.01	-10.51	309 (35)	1.03
3	Cellulose-3	*R*-*S*	-388.72	-0.61	-206.85	637 (364)	2.14
	Cellulose-1	*S*-*R*	-652.99	-1.91	-83.52	342 (69)	1.15
4	Cellulose-3	*S*-*R*	-218.37	-0.20	-158.74	1092 (819)	3.66
	Cellulose-1	*R*-*S*	-2208.67	-6.57	-249.82	336 (63)	1.13
5	Cellulose-3	*R*-*S*	-1805.12	-5.22	-248.78	346 (73)	1.16
	Cellulose-1	*S*-*R*	-20.21	0.18	-73.88	--	--
7	Cellulose-3	X_7-Y_7	-1187.26	-3.25	-218.27	365 (92)	1.22
	Cellulose-1	--	0	0	0	--	--
8	Cellulose-3	X_8-Y_8	-637.06	-1.65	-145.11	386 (113)	1.29
	Cellulose-1	X_8-Y_8	-282.78	-0.87	-23.39	325 (52)	1.09
9	Cellulose-3	*R*-*S*	-378.19	-0.97	-88.98	390 (117)	1.31
	Cellulose-1	*S*-*R*	-285.91	-0.74	-65.28	386 (113)	1.30

769 Abbreviation: EEO, enantiomer elution order; Fc, ferrocene; T_{iso}, isoenantioselective temperature; Q,
770 thermodynamic ratio

771

Table 2. Thermodynamic parameters calculated from the van't Hoff plots (temperature range 278.15-313.15 K) for the enantioseparation of ferrocenes **1**-**9** on the Lux Cellulose-3 with MeOH/water 90:10 v/v as a MP (flow rate, 0.8 ml/min). The thermodynamic parameters calculated for the enantioseparation of ferrocenes **1**-**3** and **7**-**9** [5], and **4**-**6** on the Lux Cellulose-1 are reported for comparison

Fc	Column	EEO	ΔΔH (cal/mol)	ΔΔS ($cal.K^{-1}.mol^{-1}$)	ΔΔG (cal/mol)	T_{iso}, K (°C)	Q
1	Cellulose-3	*R*-*S*	-228.25	-0.40	-108.99	571 (297)	1.91
	Cellulose-1	--	0	0	0	--	--
2	Cellulose-3	*R*-*S*	-658.95	-1.16	-313.10	568 (295)	1.90
	Cellulose-1	*S*-*R*	-311.77	-1.07	-12.75	310 (37)	1.04
3	Cellulose-3	*R*-*S*	-685.08	-1.16	-339.23	591 (317)	1.98
	Cellulose-1	*S*-*R*	-206.03	-0.55	-42.05	375 (101)	1.26
4	Cellulose-3	*S*-*R*	-570.51	-1.03	-263.42	554 (281)	1.86
	Cellulose-1	*R*-*S*	-378.67	-1.05	-65.61	361 (87)	1.21
5	Cellulose-3	*R*-*S*	-1187.09	-3.82	-48.16	311 (38)	1.04
	Cellulose-1	*S*-*R*	-359.30	-0.94	-79.04	382 (109)	1.28
6	Cellulose-3	*S*-*R*	-710.31	-1.59	-236.25	447 (174)	1.50
	Cellulose-1	*R*-*S*	-289.03	-0.81	-47.53	357 (84)	1.20
7	Cellulose-3	X_7-Y_7	-502.48	-0.88	-240.11	571 (297)	1.91
	Cellulose-1	--	0	0	0	--	--
8	Cellulose-3	X_8-Y_8	-472.43	-0.89	-207.08	531 (258)	1.78
	Cellulose-1	X_8-Y_8	-197.11	-0.56	-30.14	352 (79)	1.10
9	Cellulose-3	*R*-*S*	-417.37	-0.86	-160.96	485 (212)	1.63
	Cellulose-1	*S*-*R*	-89.80	-0.30	-0.35	299 (25)	1.00

Abbreviation: EEO, enantiomer elution order; Fc, ferrocene; T_{iso}, isoenantioselective temperature; Q, thermodynamic ratio

Table 3. Interaction energies (E_{int}) (kcal/mol) and component contributions (E_{el}, E_{vdW}) for the association of (*R*)-**3** and (*S*)-**3** with CDMPC (EEO_{exp} = *S*-*R*) and CMB (EEO_{exp} = *R*-*S*)

CDMPC				CMB			
EEO_{calc}	E_{int}	E_{el}	E_{vdW}	EEO_{calc}	E_{int}	E_{el}	E_{vdW}
S	-20.54	-5.28	-15.26	*R*	-25.83	-7.09	-18.74
R	-23.62	-6.32	-17.30	*S*	-32.74	-9.22	-23.52